Historical Changes in the Beaufort–Chukchi–Bering Seas Surface Winds and Waves, 1971–2013

XIAOLAN L. WANG, YANG FENG, AND VAL R. SWAIL

Climate Research Division, Science and Technology Branch, Environment Canada, Toronto, Ontario, Canada

ANDREW COX

Oceanweather, Inc., Cos Cob, Connecticut

(Manuscript received 11 March 2015, in final form 20 May 2015)

ABSTRACT

This study characterizes historical changes in surface wind speed and ocean surface waves in the Beaufort–Chukchi–Bering Seas using Environment Canada's Beaufort Wind and Wave Reanalysis for the period 1970–2013. The results show that both the significant wave height (H_s) and mean wave period (T_m) have increased significantly over the Bering Sea in July and August and over the Canadian Beaufort Sea westward to the northern Bering Sea in September, and that the 1992–2013 trends in September mean H_s agree well with satellite-based trend estimates for 1993–2010. Most outstandingly, the regional mean T_m has increased at a rate of 3%–4% yr^{-1} of the corresponding 1970–99 climatology; it has more than tripled since 1970. Also, the regional mean H_s has increased at a rate of 0.3% to 0.8% yr^{-1}. The trends of lengthening wave period and increasing wave height imply a trend of increasing wave energy flux, providing a mechanism to break up sea ice and accelerate ice retreat. The results also show that changes in the local wind speeds alone cannot explain the significant changes in waves. The wind speeds show significant increases over the Bering Sea to the north of Alaska in July and over the central part of the domain in August and September, with decreases in the region off the Canadian coasts in August. In the region west of the Canadian coast, the climatological mean wind direction has rotated clockwise in July and August, with the climatological anticyclonic center being displaced northeastward in August.

1. Introduction

The Arctic sea ice extent has been decreasing under global warming. According to IPCC (2013), the annual mean Arctic sea ice extent decreased over the period 1979–2012 with a rate that was very likely in the range 0.45 to 0.51 million km^2 decade^{-1}, and very likely in the range 0.73 to 1.07 million km^2 decade^{-1} for the summer sea ice minimum (perennial sea ice). The IPCC (2013) concluded with high confidence that the average decrease in decadal mean extent of Arctic sea ice has been most rapid in summer, and that the spatial extent has decreased in every season, and in every successive decade since 1979. Satellite observation records show substantial losses in Arctic sea ice, particularly at the time of the minimum extent, which occurs in September at the end of the annual melt season (Hartmann et al. 2013). It is very likely that the Arctic sea ice cover will continue to shrink and thin during the twenty-first century as global mean surface temperature rises (IPCC 2013). Decreased sea ice extent opens the ocean surface up for wind-wave generation, exposing a greater coastal/offshore area to impacts of ocean surface waves (e.g., coastal erosion, shoreline sediment transportation), among other opportunities (e.g., shipping) and impacts [see Stephenson et al. (2011) for examples]. Since open water distances are the controlling variable for wave heights in the Beaufort–Chukchi–Bering (BCB) Seas, larger waves and more common swells are to be expected under scenarios for reduced seasonal sea ice cover, and the increased wave activity could be one feedback mechanism that drives the Arctic system

Denotes Open Access content.

Corresponding author address: Xiaolan L. Wang, Climate Research Division, Science and Technology Branch, Environment Canada, 4905 Dufferin Street, Toronto, ON M3H 5T4, Canada.
E-mail: xiaolan.wang@ec.gc.ca

DOI: 10.1175/JCLI-D-15-0190.1

toward an ice-free summer (Thomson and Rogers 2014). All these indicate that scientific information about and assessment of the climate, trends, and variability of the Arctic Ocean surface waves are important for climate change projections and climate prediction on the global and regional scales, and for adaptation and migration of climate change in the Arctic region, among many other applications. However, such information scarcely exists. There is an emerging need to study surface waves in the emerging Arctic Ocean.

However, because of a lack of wave data, there exist few studies on long-term historical changes in ocean surface waves in the Arctic, especially in the BCB Seas. Recently, Francis et al. (2011) analyzed cross-validated satellite altimeter radar observations for the period 1993–2011 and showed a strong trend of increasing surface wave heights in the Arctic Ocean, with the highest trends of up to 0.03–0.04 m yr^{-1} near the northern Alaskan coast (usually located 100–200 km offshore).

As described in Swail et al. (2007), Environment Canada produced the first comprehensive high-resolution wind and wave reanalysis for this region, namely the MSC (Meteorological Service of Canada, Environment Canada) Beaufort Wind and Wave Reanalysis, initially for the period 1985–2005. This wind and wave reanalysis has been extended to span the period 1970–2013 and is being updated to the present. Since buoy wave observations are limited to a number of buoy sites, and satellite wave observations to the recent couple of decades, wave reanalysis data have been used to analyze historical trends in waves (e.g., Semedo et al. 2011; Wang and Swail 2001, 2002). This study aims to use the MSC Beaufort Wind and Wave Reanalysis data to characterize the climate and trends of wind and waves in the BCB Seas.

The remainder of the paper is arranged as follows. The data and methodology used in this study are described in sections 2 and 3, respectively. Historical changes in wind speed and waves (significant wave height and mean wave period) are presented in sections 4 and 5, respectively. A summary in section 6 completes this study.

2. Data

The wind and wave data analyzed in this study, including surface wind speed (W_s), wind direction (W_d), significant wave height (H_s), and mean wave period (T_m), are taken from an updated version of the MSC Beaufort Wind and Wave Reanalysis [originally described by Swail et al. (2007)] for the period 1970–2013. Data are available for a coarse domain including the BCB domain [66°–76°N (originally 60°–76°N), 140°E–110°W] and a fine Canadian Beaufort Sea domain. The spatial resolution is roughly 28 km (on a 0.25° × 0.75° lat/lon grid) for the coarse BCB domain and roughly 5.2 km (on a 0.05° × 0.15° lat/lon grid) for the fine Beaufort Sea domain. Although we analyzed data for both the coarse and fine domains, we present our results for the coarse domain only, noting no marked differences in trends for the fine domain (this is because model resolution would affect the absolute values of wave parameters much more than the trends therein; its effect on trends is minimal, especially when trends are expressed in percentage of the climatological mean values).

As detailed in Swail et al. (2007), the wind fields were analyzed using the Interactive Objective Kinematic Analysis (IOKA) system of Oceanweather Inc. (OWI) (Cox et al. 1995). In the wind analysis, all available measured wind data were brought into a background field and assimilated at 6-hourly intervals with the guidance and input of an experienced kinematic analyst working through a graphical interactive tool called the Wind WorkStation. The coastal stations measurements of wind speed were transformed to effective overwater exposure at 10-m elevation, using the station-dependent overwater/overland transformation ratios derived from station surface roughness and anemometer height. The background wind field is taken from the 10-m surface wind-gridded products of the NCEP–NCAR reanalysis (NRA; Kalnay et al. 1996), which covers the period 1948 to the present. The global QuikSCAT wind database (http://manati.star.nesdis.noaa.gov/products/QuikSCAT.php) was used to identify and correct systematic errors in the NRA winds within the domain of the ocean response models.

The wave fields were produced by using the above analyzed wind fields to drive the Oceanweather third-generation (OWI-3G) wave model, with boundary spectra of the basin model being supplied from the GROW (Global Reanalysis of Ocean Waves) hindcast (Swail et al. 2007). The physics of the OWI-3G model are described in Khandekar et al. (1994). The General Bathymetric Chart of the Oceans (GEBCO) provided water depths for most of the basinwide hindcast; depths for the fine grid as well as overlapping regions of the coarse grid were supplied from the Canadian Hydrographic Service (CHS) archive. The two datasets were found to be consistent, so little smoothing was required at their boundary. Grid boxes with greater than 50% ice concentration are considered as land with no wave generation and/or propagation. This simple treatment of ice was implemented in the model because this wave reanalysis was produced prior to much of the most recent developments in the wave–ice interactions. In the

coarse BCB domain the ice edge was allowed to change on a weekly basis to represent changing ice conditions during transition periods. The ice concentration data sources include the Goddard Space Flight Center (GFSC) daily data for the BCB domain for November 1970 to December 2000, the Defense Meteorological Satellite Program (DMSP) daily data for the BCB domain for January 2001 to the present (2013), and the Canadian Ice Service (CIS) weekly high-resolution ice concentration dataset for Canadian waters for the period since January 1970.

Swail et al. (2007) validated the MSC Beaufort Wave Reanalysis with the wave measurements from the 12 MEDS (Marine Environmental Data Service) buoys in the Canadian Beaufort for the period 1981–86. They concluded that overall the wave reanalysis reflects the measured day-to-day and storm conditions, although both under- and overestimation are seen in the reanalysis. For 32 storm peaks, the reanalysis shows on average an underestimation of 22 cm in wave height and of 1.05 s in wave period (Swail et al. 2007). For events of greater than 2-m H_s, the reanalysis shows on average an underestimation of 21 cm (8.6%) in H_s and of 0.56 s (7.4%) in wave period, as derived from data in Fig. 9 of Swail et al. (2007).

3. Methodology

As shown in Fig. 1, during the period 1970–2013, the open water exists in the BCB domain only in July to September (with a few grid boxes of open water in October; not shown), and the area of wave data (open water) increases considerably from July to September (larger increases from July to August than from August to September). Thus, we carried out our analysis for July, August, and September, separately.

Considering that the open water area in the BCB domain increased more notably between the last two decades than between the earlier decades (Fig. 1a) and has remarkable interannual variations (Fig. 1b), we characterize trends in three ways. First, we show the 1970–91 and 1992–2013 climatological mean fields of each variable analyzed for each of the three months, and the changes between these two 22-yr periods (Figs. 2–5). Second, we derive the regional mean time series of each variable for each of the three months and estimate trends in these time series (Fig. 6). Note that in each calendar month the sampling region for the regional mean time series increases over time and changes from year to year (Fig. 1b). Third, we estimate trends at each wave grid point for the periods 1971–2013 and 1992–2013 to show the spatial patterns of trend (Fig. 7).

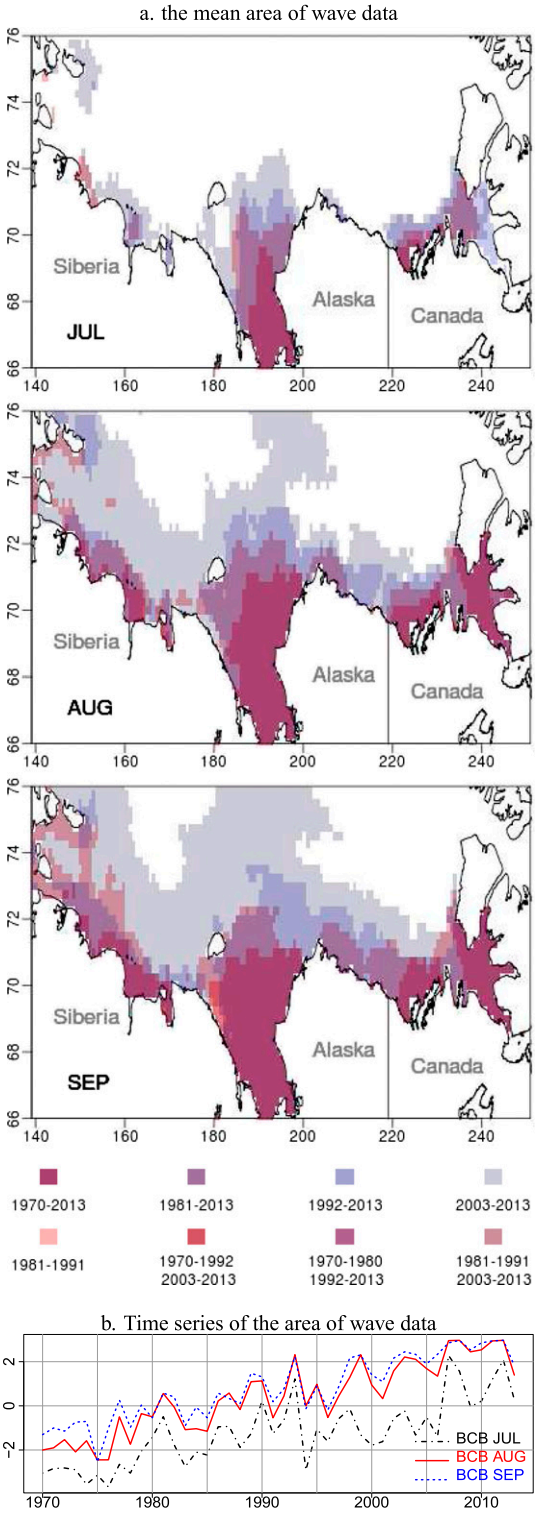

FIG. 1. (a) The mean area of wave data (open water) in the indicated months over the indicated periods. (b) The standardized time series of the area of wave data in the Beaufort–Chukchi–Bering (BCB) Seas domain for July, August, and September. The three time series were standardized using the same mean and standard deviation, which were derived from pooling the three time series together. Thus, the differences between these time series are proportional to the differences in the area of open water between the three months.

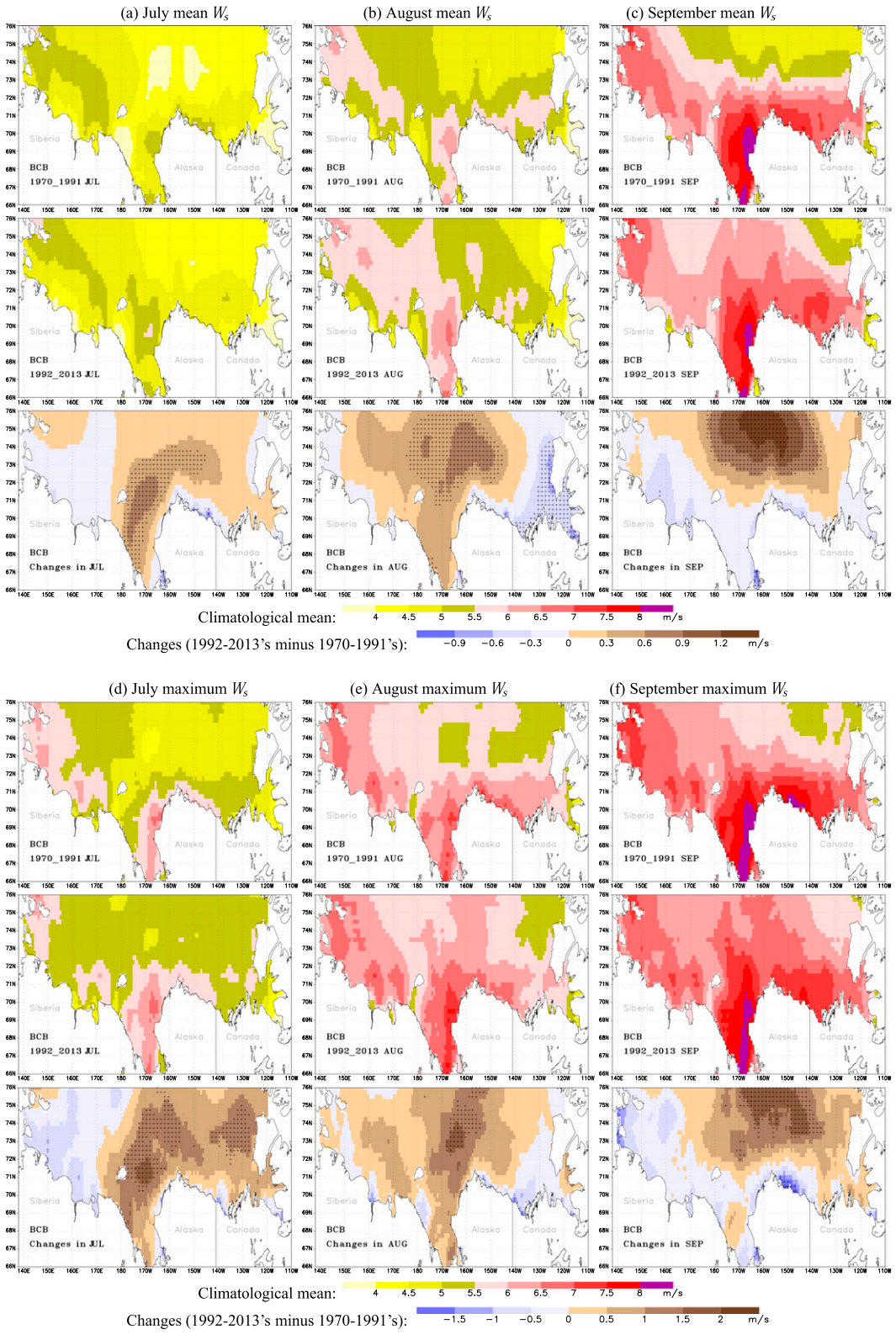

FIG. 2. The climatological (1970–91 and 1992–2013) means of monthly mean and maximum wind speed (W_s) in the indicated month over the BCB Seas domain, and the changes between the two 22-yr periods (1992–2013 minus 1970–91). Stippling indicates areas where the changes are significant (at 5% level).

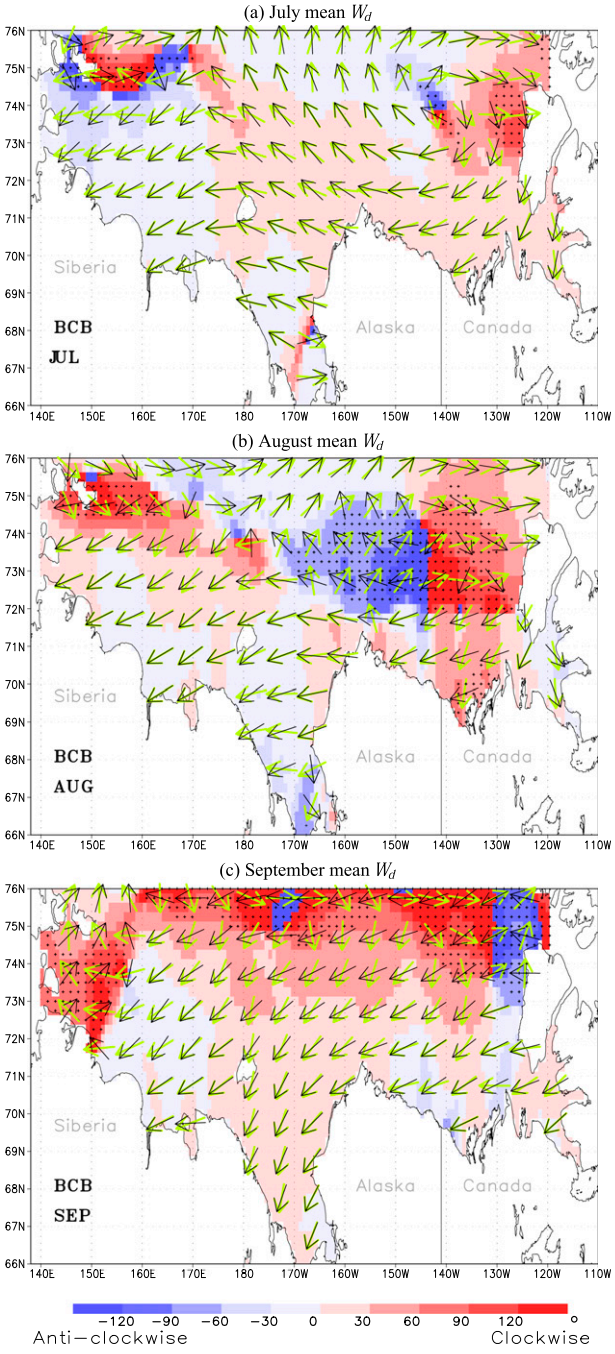

FIG. 3. Maps of the climatological mean wind directions (W_d) for the periods 1970–91 (green arrows) and 1992–2013 (black arrows), and the changes in the mean W_d between these two periods (shading). Stippling indicates areas where the changes are significant (at 5% level).

We analyzed monthly mean and maximum values of wind speed (W_s) and significant wave height (H_s), as well as monthly means of wind direction (W_d), mean wave period (T_m), and wave age (W_a). Here, the wave age is derived using the monthly mean W_s and monthly mean T_m: $W_a = 1.56T_m/W_s$, with T_m in units of seconds and W_s in m s^{-1}. The climatological mean fields of H_s and T_m are shown for grid points that have wave data for the calendar month being analyzed throughout the corresponding climatological period (1970–91 or 1992–2013). This is necessary since the area of wave data (open water) in the BCB domain increases over time as the Arctic sea ice retreats under global warming; that is, the area of open water is smaller in the early years than in the more recent years (Fig. 1). The regional mean time series of the 90th and 99th percentiles of W_s and H_s were also derived and subjected to trend analysis. Note that we derived the regional mean time series of W_s as averages over the entire BCB domain, and over only the grid points of wave data (same grid points as for the H_s and T_m series), to provide insight into how local and remote winds contribute to changes in waves.

Considering that wind speeds, wave heights, and mean wave periods are nonnegative nonnormal data, we used the trend analysis method of Wang and Swail (2001), which is a Mann–Kendall estimator and test (Kendall 1970; Mann 1945) that accounts for the effect of lag-1 autocorrelation on trend estimates and has been found to perform best in comparison with other trend calculation methods (Hartmann et al. 2013; Zhang and Zwiers 2004). The Mann–Kendall estimator is based on ranks (nonparametric) and is thus less vulnerable to gross errors and the associated confidence interval is less sensitive to nonnormality of the parent distribution than the commonly used least squares estimator. The trend estimates in Figs. 6 and 7 (upper panels) are for the 43-yr period 1971–2013 (instead of the 44-yr period 1970–2013 because of accounting for lag-1 autocorrelation). The results are discussed in the next section.

4. Trends in surface wind speed

Figure 2 shows the climatological mean fields of monthly mean and maximum wind speeds for the two 22-yr periods, 1970–91 and 1992–2013, and the changes between these two periods. During July–September, the climatological highest wind speeds over the domain are seen in the Bering Sea (just west of Alaska); the climatological mean wind speeds increase from July to September (Fig. 2).

There were significant changes in the climates of wind speeds from the first to the second period, as shown in Fig. 2. The climatological mean of monthly mean wind speeds increased significantly from the first to the second period over the Bering Sea to north of Alaska in July, over the central part of the domain in August and September, but decreased in the region off the Canadian coasts in August (Fig. 2). The climate of monthly

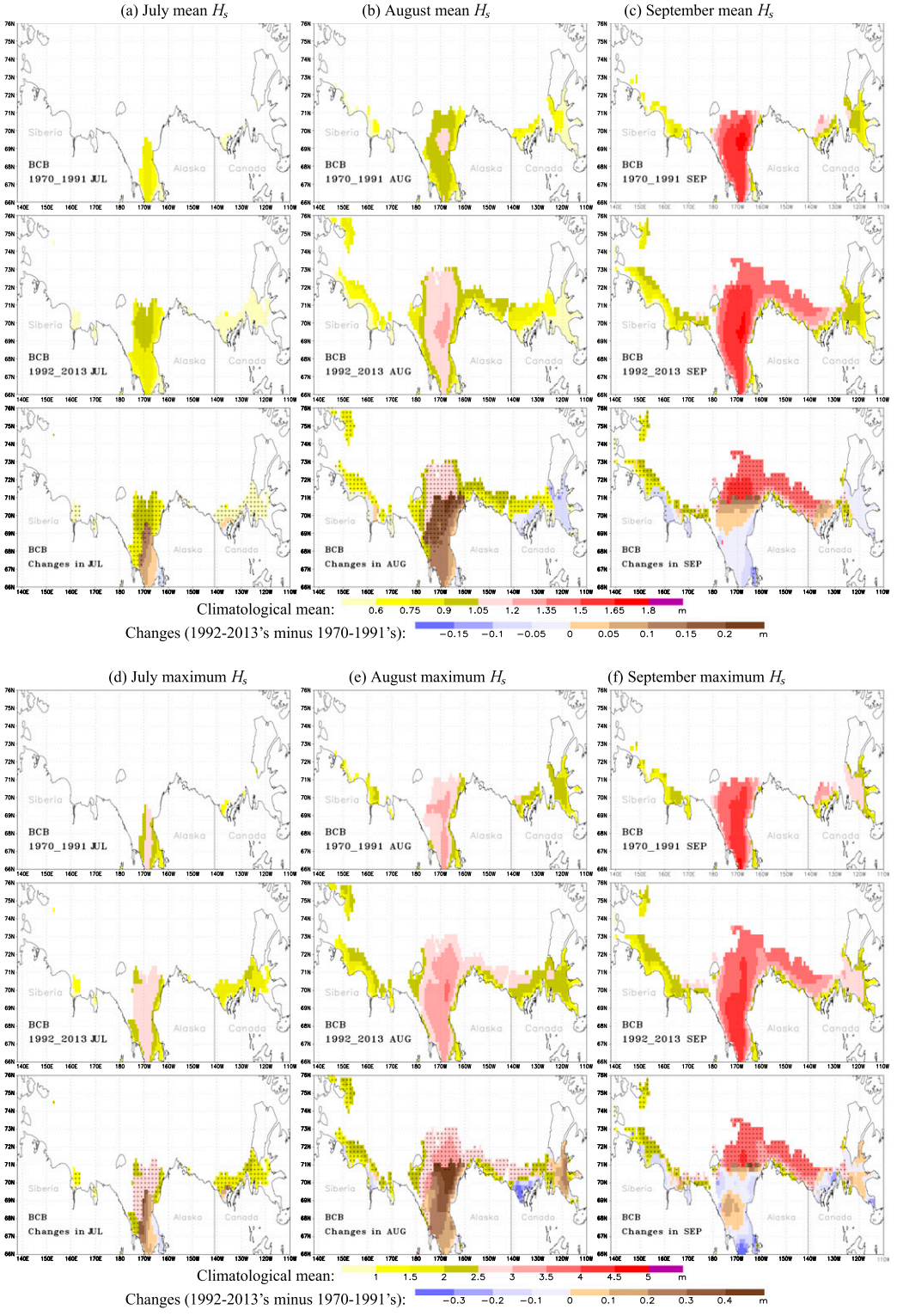

FIG. 4. The climatological (1970–91 and 1992–2013) means of significant wave height (H_s) in the indicated month over the BCB Seas domain, and the changes between the two 22-yr periods (1992–2013 minus 1970–1991). In the areas where open water existed only in the second period, the climatological mean of the second period is shown. Stippling indicates areas where the changes are significant (at 5% level).

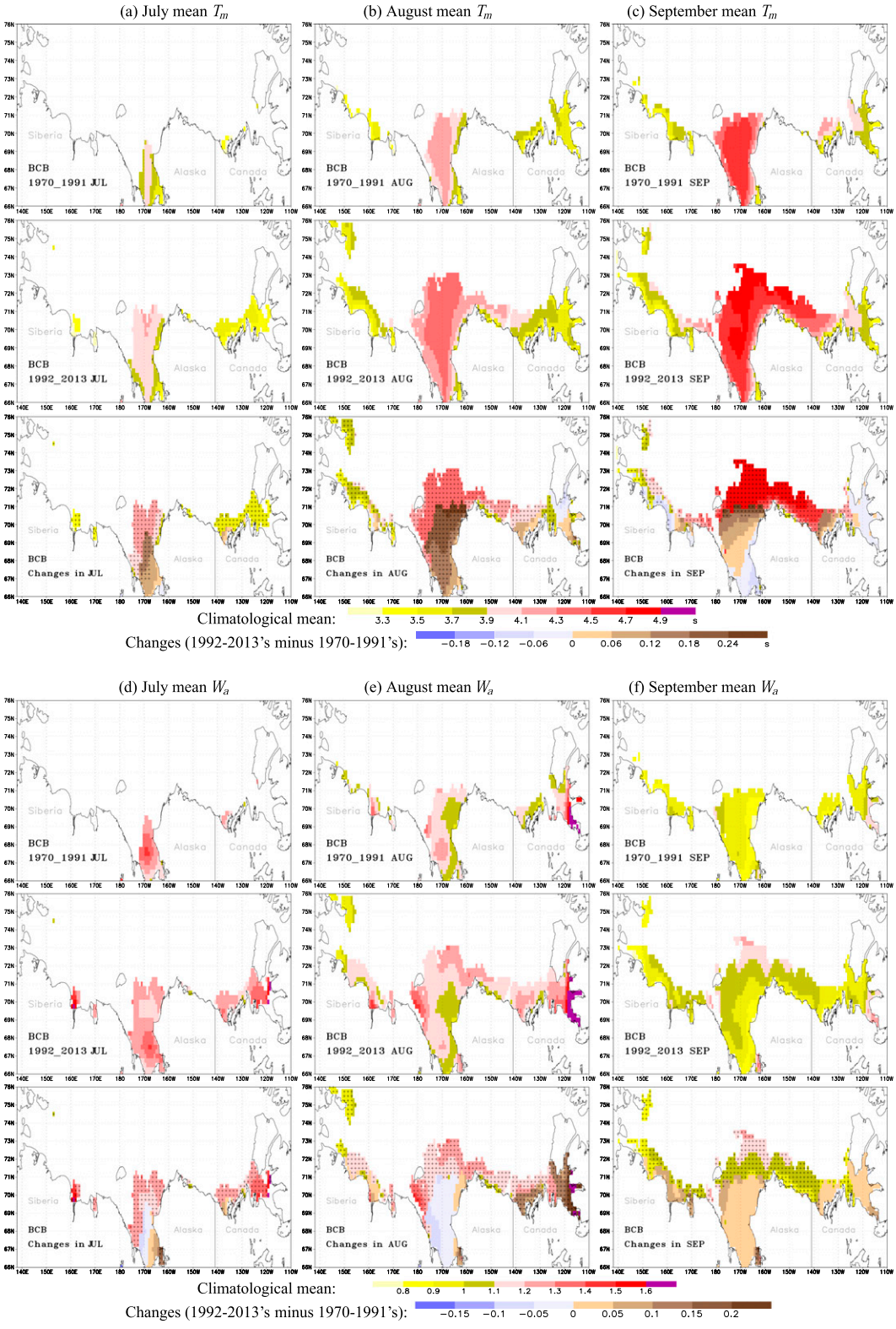

FIG. 5. As in Fig. 4, but for the climatological (1970–91 and 1992–2013) means of mean wave period (T_m) and wave age (W_a) in the indicated month over the BCB Seas domain, and the changes between the two 22-yr periods (1992–2013 minus 1970–91).

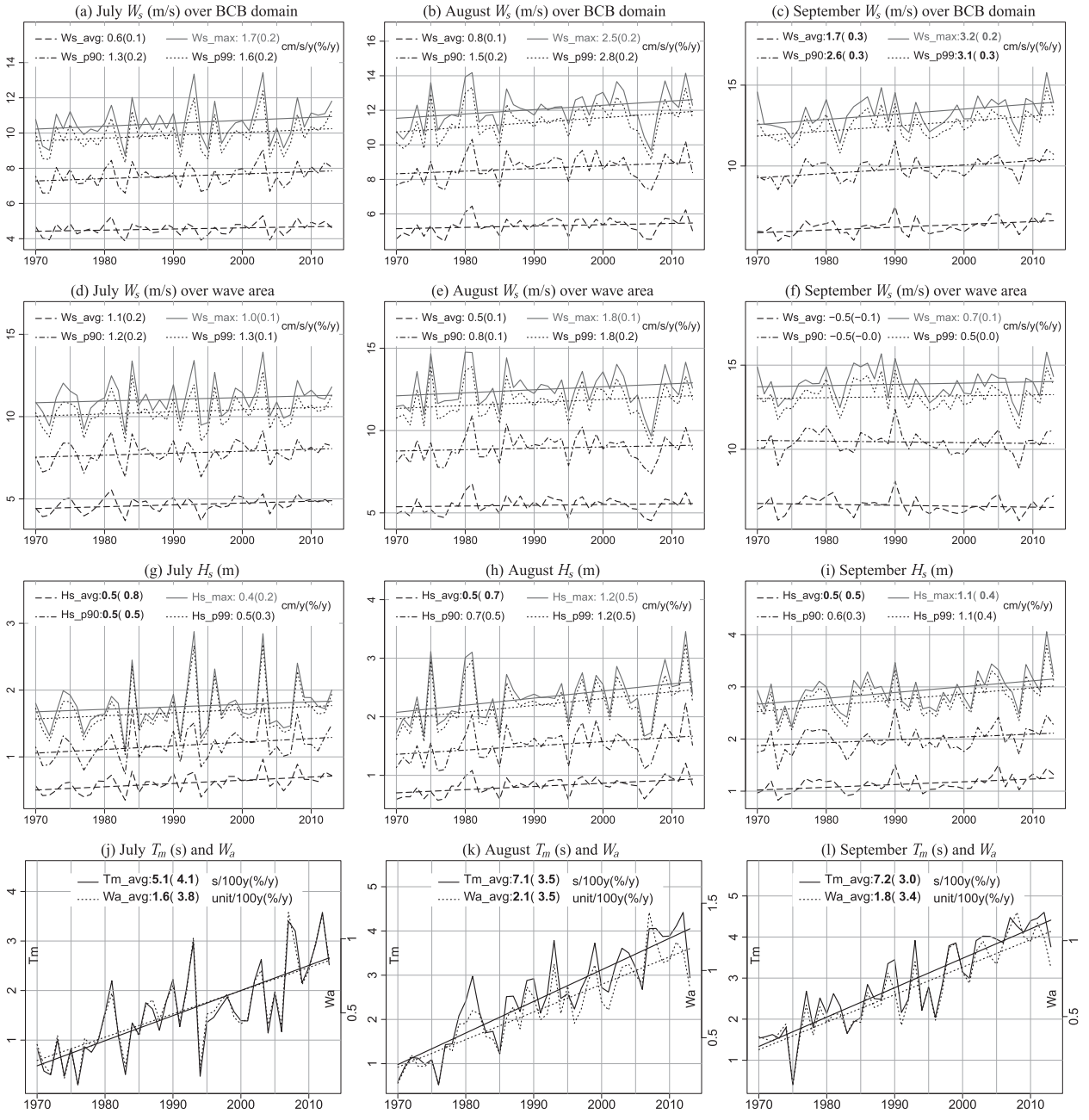

FIG. 6. The regional mean time series of wind speed (W_s), significant wave height (H_s), mean wave period (T_m), and wave age (W_a). Here, "avg," "p90," "p99," and "max" denote the monthly mean, 90th percentile, 99th percentile, and maximum of the variable in question, respectively. The trend estimates are also expressed in percentage of the 1970–99 climatological mean (the numbers in parentheses). Trends of 5% significance or higher are shown in bold. Note that the regional mean time series of W_s over wave area (in second row) are averages over only the grid points of wave data (same grid points as for the H_s, T_m, and W_a series).

maximum wind speeds show similar changes, except in the region off the Canadian coasts where significant increases are seen only in July maximum wind speeds and significant decreases are seen only in August mean wind speeds (Fig. 2).

As shown in Fig. 3, the climatological mean wind direction also varies notably from July to September, and there are also notable changes in the mean wind direction between the two 22-yr periods, especially in the eastern part of the domain in August and in the northern part in September (Fig. 3). In the area west of the Canadian coast, the July and August mean wind direction has rotated clockwise, with the climatological anticyclonic center seen in this region in August being

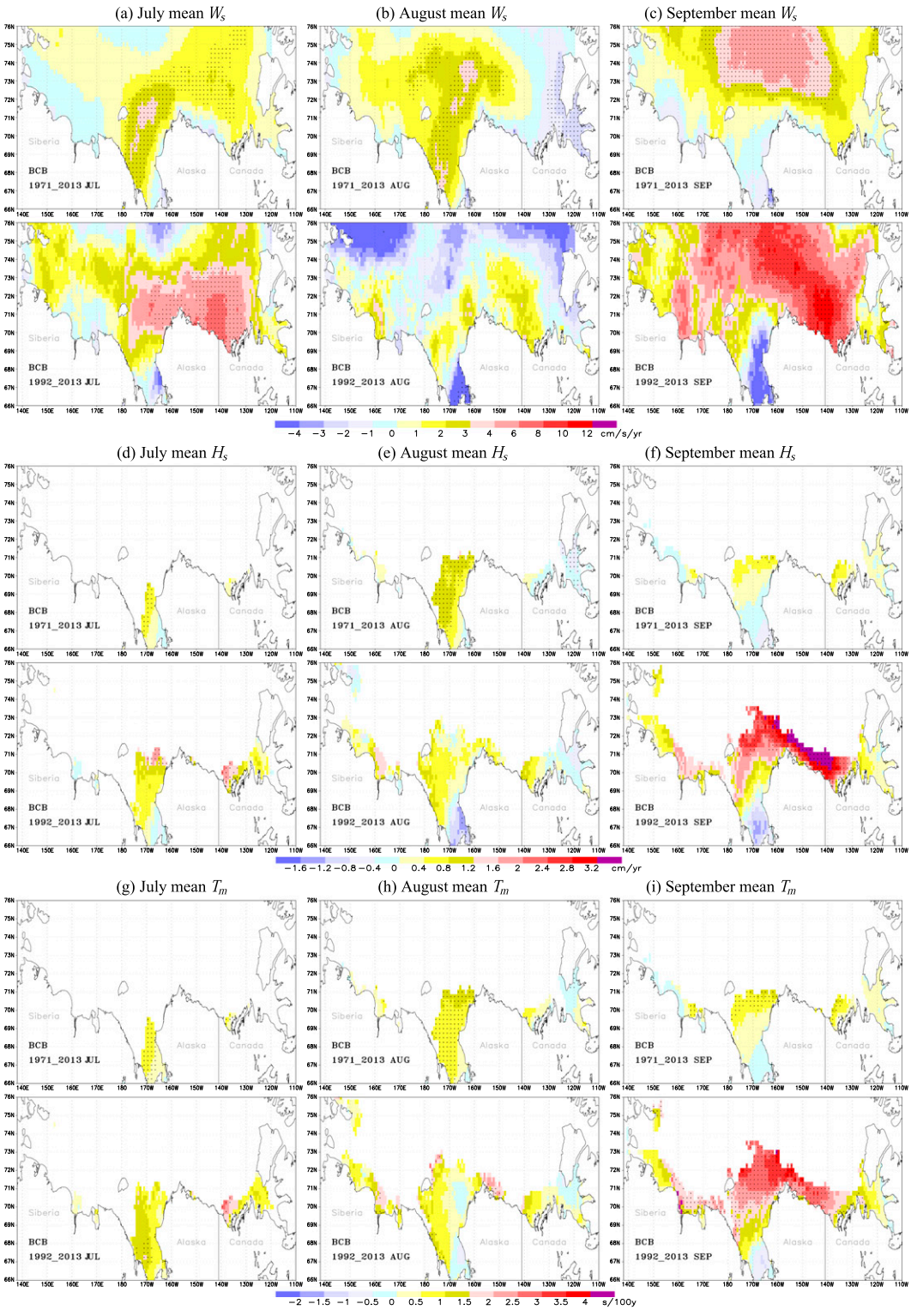

FIG. 7. Maps of 1971–2013 and 1992–2013 linear trends in the indicated monthly mean wind speed (W_s), significant wave heights (H_s), and mean wave period (T_m) over the BCB Seas domain. Stippling indicates areas where the trends are significant (at 5% level).

displaced from near the Alaskan north coast (71.5°N, 152°W) northeastward to around 74°N, 142°W. Another anticyclonic center can be seen in the first period in the region north of the western Siberia, around 75.5°N, 155°E in September, which shows northeastward displacement to north of 76°N in the second period.

The regional mean time series of the four monthly statistics (mean, 90th percentile, 99th percentile, and maximum) of wind speeds, along with the estimates of their 1971–2013 trends, are shown in Figs. 6a–f. Averaged over the entire BCB domain (Figs. 6a–c), all the four statistics of wind speeds show an increasing trend in each of the three months, but the increasing trends are statistically significant (at 5% level) only in September. When expressed in percentage of the corresponding 1970–99 climatological mean, the increases range from 0.1% to 0.3% yr^{-1}. In July and August, the monthly maximum wind speed appears to have greater percentage increases than does the monthly mean, but the opposite is seen in September (Figs. 6a–c, numbers in parentheses). Averaged over the area of waves (open water) (Figs. 6d–f), the wind speed trends are statistically not significant for all statistics in all the three months.

There are also notable spatial variations of trends in wind speed W_s, and the trend patterns are different in different calendar months and also in different periods (Figs. 7a–c). In July, the 1971–2013 trend pattern of monthly mean W_s is characterized by significant increases in the region west and north of the Alaskan coast, extending to the Canadian Beaufort; larger increases are estimated for the period 1992–2013, in which the area of significant W_s increases extended to the Alaska nearshore area (Fig. 7a). For August mean W_s, the 1971–2013 trends show significant increases in the central part, with significant decreases in the eastern part of the domain, but there is no significant trend in August mean W_s over the past 22 years (Fig. 7b). In September, the 1971–2013 trend pattern of monthly mean W_s is characterized by significant increases in the central-north part of the domain; larger increases were also estimated for the period 1992–2013, in which the area of significant W_s increases extended south to the Canadian and Alaskan north coast (Fig. 7c). The monthly mean and maximum W_s share similar patterns of trends, with the monthly maximum W_s showing less extensively significant trends in general (not shown).

5. Trends in ocean surface waves

In this section, we present trends in four monthly statistics (mean, 90th percentile, 99th percentile, and maximum) of significant wave heights (H_s), and in monthly mean wave period (T_m) and monthly mean wave age (W_a).

For the two 22-yr periods, 1970–91 and 1992–2013, the climatological mean fields of monthly mean and maximum H_s, monthly mean T_m, and monthly mean W_a are shown along with the changes between these two periods in Figs. 4 and 5. Note that only the grid points that have wave data throughout the entire analysis period (1970–91 or 1992–2013) are included here and throughout this study. For the new area of waves and/or open water (which is open water only in the second period), the changes in the climatological means between the two periods are equal to the climatology of the second period and deemed to be statistically significant in comparison to the climatology of the first period.

It is worth noting that because the wave grid is truncated at 76°N and thus does not account for wave growth north of this region, it is possible that the climatological values of H_s, T_m, and W_a are underestimated in the wave reanalysis analyzed in this study.

As shown in Fig. 4, the area of waves increased notably from the first to the second period, with larger increases in August and September than in July. In July, the area of waves is limited to the southern Bering Sea in the 1971–92 period; it extends northward to about 72°N and emerges in the Canadian Beaufort Sea since early 1990s (Fig. 4a). In August and September, the area of waves exists in the Canadian Beaufort Sea throughout the reanalysis period (1970–2013) and extends northwestward in the Bering Sea (Figs. 4b,c).

During July–September, the climatological highest H_s and longest T_m over the domain are seen in the Bering Sea (just west of Alaska); the climatological mean H_s and T_m increase from July to September (Figs. 4 and 5). These climatological features are generally consistent with those seen in the surface winds. The area of the climatological highest H_s and longest T_m is generally determined by the climates of wind speeds, wind direction, and the fetch distance (open water area along the wind direction), and modified by the bathymetric details, coastlines, and sea ice edges. As shown in Figs. 5d–f, the wave age, which is proportional to the ratio of wave period and wind speed, shows high values in the western Bering Sea, but the highest climatological values are seen off the Canadian coast, where the wave age is probably not as well estimated using the formula for deep waters (a shallow or transitional water formula would fit better, which we will explore in a future study).

There were significant changes in the H_s, T_m, and W_a climates from the first to the second period, as shown in Figs. 4 and 5. The climatological means of monthly mean H_s and T_m have increased significantly from the first to the second period over the Bering Sea in July and

August, and over the area from the Canadian Beaufort westward to the northern Bering Sea in September (Figs. 4a–c and 5a–c). The climate of monthly maximum H_s shows similar changes, except that the H_s increases in the Bering Sea in August are only statistically significant for the monthly mean H_s (Fig. 4). The significant changes in wave age are mainly in the new open water area (Figs. 5d–f), except in the region off the Canadian coast in August where the wave age is not as well estimated, as explained above.

The regional mean time series of the four monthly H_s statistics, along with the estimates of their 1971–2013 trends, are shown in Figs. 6g–i. The monthly mean H_s was found to have increased significantly (at 5% level) in each of the three calendar months since 1970, and so were the July 90th percentiles and the September maximum of H_s. The other H_s statistics also show an increasing trend but are not statistically significant. When expressed in percentage of the corresponding 1970–99 climatological mean, the increases range from 0.3% to 0.8% (0.5 to 1.1 cm) yr^{-1}, and the monthly mean H_s appears to have greater percentage increases than does the corresponding monthly maximum (Figs. 6g–i).

The regional mean monthly mean wave period (T_m) has increased significantly in all the three calendar months since 1970, showing increases of 3.0% to 4.1% yr^{-1} (5.1 to 7.2 s century^{-1}), with the highest percentage increase seen in July (Figs. 6j–l). The July, August, and September climatological means of regional mean wave period have increased from around 0.5, 1.0, and 1.3 s in year 1970 to around 2.6, 4.0, and 4.4 s in year 2013, respectively. In other words, the mean wave period has more than tripled since 1970. These are the most significant changes seen in the BCB wave climate.

Changes in the local wind speeds alone cannot explain the significant trends in waves (H_s and T_m) because the regional mean wind speeds averaged over the area of waves (open water) show no significant trends (Figs. 6d–f). In this case, the monthly mean wave age shares a similar trend with the corresponding mean wave period (Figs. 6j–l). This indicates the important roles of swells, which are generated by nonlocal winds, and of the breaking up of Arctic sea ice, which increased fetch lengths and contributed to longer wave periods and taller waves. Changes in the climatological wind direction could also contribute to changes in waves.

As shown in Figs. 7d–i, there are notable spatial variations of trends in H_s and T_m, and the trend patterns also vary from July to September. In July, the wave height H_s has increased significantly in the west edge of the wave area in the southern Bering Sea since 1971, and in the northern edge of the wave area (i.e., the new area of waves) in the past two decades (Fig. 7d). In August, the wave heights show significant increases in the Bering Sea and significant decreases in the eastern part of the Canadian Beaufort since 1971, but no significant trend over the past two decades (Fig. 7e). In September, the wave heights show no significant trend in the area of waves throughout the 44-yr period since 1970; however, significant increases of up to about 4 cm yr^{-1} are seen in the new area of waves over the period 1992–2013 (Fig. 7f). The monthly mean wave period shares similar trend patterns with the corresponding monthly mean H_s, although it shows more extensively significant increases than does the monthly mean H_s (Figs. 7d–i).

The 1992–2013 trend estimates for September mean H_s are in good agreement with the satellite-based trend estimates by Francis et al. (2011), although the sampling season, the period of analysis, and trend analysis method are different [their sampling season is 35 days in summer, the period of analysis is 1993–2010, and trend analysis method is (least squares) linear fit].

Since wave energy flux is proportional to the product of mean wave period and squared H_s, increases in both wave period and H_s imply increases in wave energy flux, which in turn provide a mechanism to break up sea ice and accelerate ice retreat (Kohout et al. 2014; Thomson and Rogers 2014).

6. Summary and discussion

We have analyzed the historical trends/changes in surface wind speed and ocean surface waves in the Beaufort–Chukchi–Bering (BCB) Seas using the MSC Beaufort Wind and Wave Reanalysis for the period 1970–2013. Considering the changing open water area, we characterize trends in terms of changes in climatological mean fields between two subperiods (1970–91 and 1992–2013), as well as trends in the regional mean time series of each variable for July, August, and September, separately. The 1971–2013 and 1992–2013 trends at each wave grid point were also estimated to show the spatial patterns of trend.

The results show that the climatological means of monthly mean H_s and T_m have increased significantly from the period 1970–91 to the period 1992–2013 over the Bering Sea in July and August, and over the area from the Canadian Beaufort westward to the northern Bering Sea in September (Figs. 4a–c and 5a–c). In July, the area of waves (open water) extends from the southern Bering Sea northward to about 72°N and emerges in the Canadian Beaufort Sea during the past two decades (Fig. 4a). In August and September, the area of waves exists in the Canadian Beaufort Sea throughout the reanalysis period (1970–2013) and extends northwestward in the Bering Sea (Figs. 4b,c).

Significant increases were also identified in the September wave heights and mean wave periods in the new area of waves over the recent two decades (1992–2013). The 1992–2013 trend estimates for September mean H_s are in good agreement with the satellite-based trend estimates for the period 1993–2010 (Francis et al. 2011).

This study also shows that the regional mean of monthly mean H_s has increased significantly in each of the three calendar months, as did the July 90th percentiles and the September maximum of H_s. The rates of increase in the regional mean H_s range from 0.3% to 0.8% $yr^{-1}$of the corresponding 1970–99 climatology. The most outstanding change in the BCB wave climate is the overwhelmingly significant lengthening of the mean wave period. The regional mean wave period was estimated to have increased at a rate of 3%–4% yr^{-1}; it has more than tripled since 1970.

The results also show that changes in the local wind speeds alone cannot explain the significant changes in waves (H_s and T_m), which indicates the important roles of swells and the breaking up of sea ice in the Arctic. The most prominent feature of changes in the wind speed climate is significant increases over the Bering Sea to north of Alaska in July, over the central part of the domain in August and September, but decreases in the region off the Canadian coasts in August (Figs. 2a–c). The climatological mean wind direction was also found to have changed notably, especially in the eastern part of the domain in August and in the northern part in September; the July and August mean wind direction rotated clockwise over the region west of the Canadian coast, with the climatological anticyclonic center seen in this region in August being displaced northeastward (Fig. 3). These changes in wind direction must have also contributed to the changes in waves.

The trend of lengthening mean wave period and increasing wave height imply a trend of increasing wave energy flux, providing a mechanism to break up sea ice and accelerate ice retreat (Thomson and Rogers 2014). This stresses the importance of studying waves in the emerging Arctic Ocean, including characterizing historical climate and trends, as well as projections of possible future wave conditions. Dynamical projections of future scenarios of wave climate in the emerging Arctic Ocean, using the surface winds simulated by phase 5 of the Coupled Model Intercomparison Project (CMIP5; Taylor et al. 2012), are currently ongoing and will be presented in a separate study.

There are other wave parameters, such as wave steepness and the fraction of swells, that are worth analyzing, especially for the changing Arctic Ocean. Currently, the Environment Canada's Beaufort Wave Reanalysis is being updated to cover the recent years. We plan to assess changes in wave steepness and in the fraction of swells in this region using an updated version of the wave reanalysis dataset.

Acknowledgments. The authors are grateful to Drs. Greg Flato and Mercè Casas-Prat for their helpful internal review of an earlier version of this manuscript. The wind and wave data (monthly statistics) analyzed in this study will be available via request made to the corresponding author: xiaolan.wang@ec.gc.ca.

REFERENCES

Cox, A. T., J. A. Greenwood, V. J. Cardone, and V. R. Swail, 1995: An interactive objective kinematic analysis system. *Proc. Fourth Int. Workshop on Wave Hindcasting and Forecasting*, Banff, AB, Canada, Atmospheric Environment Service, 109–118.

Francis, O. P., G. G. Planteleev, and V. E. Atkinson, 2011: Ocean wave conditions in the Chukchi Sea from satellite and in situ observations. *Geophys. Res. Lett.*, **38**, L24610, doi:10.1029/2011GL049839.

Hartmann, D. L., and Coauthors, 2013: Observations: Atmosphere and surface. *Climate Change 2013: The Physical Science Basis*, T. F. Stocker et al., Eds., Cambridge University Press, 159–254.

IPCC, 2013: Summary for policymakers. *Climate Change 2013: The Physical Science Basis*. T. F. Stocker et al., Eds., Cambridge University Press, 3–29.

Kalnay, E., and Coauthors, 1996: The NCEP/NCAR 40-Year Reanalysis Project. *Bull. Amer. Meteor. Soc.*, **77**, 437–471, doi:10.1175/1520-0477(1996)077<0437:TNYRP>2.0.CO;2.

Kendall, M. G., 1970: *Rank Correlation Methods.* 4th ed. Charles Griffin, 202 pp.

Khandekar, M. L., R. Lalbeharry, and V. J. Cardone, 1994: The performance of the Canadian spectral ocean wave model (CSOWM) during the Grand Banks ERS-1 SAR wave spectra validation experiment. *Atmos.–Ocean*, **32**, 31–60, doi:10.1080/07055900.1994.9649489.

Kohout, A. L., M. J. M. Williams, S. M. Dean, and M. H. Meylan, 2014: Storm-induced sea-ice breakup and the implications for ice extent. *Nature*, **509**, 604–607, doi:10.1038/nature13262.

Mann, H. B., 1945: Non-parametric tests against trend. *Econometrica*, **13**, 245–259, doi:10.2307/1907187.

Semedo, A., K. Suselj, A. Rutgersson, and A. Sterl, 2011: A global view on the wind sea and swell climate and variability from ERA-40. *J. Climate*, **24**, 1461–1479, doi:10.1175/2010JCLI3718.1.

Stephenson, S. R., L. C. Smith, and J. A. Agnew, 2011: Divergent long-term trajectories of human access to the Arctic. *Nat. Climate Change*, **1**, 156–160, doi:10.1038/nclimate1120.

Swail, V. R., V. J. Cardone, B. Callahan, M. Ferguson, D. J. Gummer, and A. T. Cox, 2007: The MSC Beaufort Wind and Wave Reanalysis. *Proc. 10th Int. Workshop on Wave Hindcasting and Forecasting and Coastal Hazard Symp.*, North Shore, Oahu, Hawaii, WMO/IOC Joint Technical Commission for Oceanography and Marine Meteorology. [Available online at http://www.waveworkshop.org/10thWaves/Papers/The%20MSC%20Beaufort%20Wind%20and%20Wave%20Reanalysis.pdf.]

Taylor, K. E., R. J. Stouffer, and G. A. Meehl, 2012: An overview of CMIP5 and the experiment design. *Bull. Amer. Meteor. Soc.*, **93**, 485–498, doi:10.1175/BAMS-D-11-00094.1.

Thomson, J., and W. E. Rogers, 2014: Swell and sea in the emerging Arctic Ocean. *Geophys. Res. Lett.*, **41**, 3136–3140, doi:10.1002/2014GL059983.

Wang, X. L., and V. R. Swail, 2001: Changes of extreme wave heights in Northern Hemisphere oceans and related atmospheric circulation regimes. *J. Climate*, **14**, 2204–2221, doi:10.1175/1520-0442(2001)014<2204:COEWHI>2.0.CO;2.

——, and ——, 2002: Trends of Atlantic wave extremes as simulated in a 40-year wave hindcast using kinematically reanalyzed wind fields. *J. Climate*, **15**, 1020–1035, doi:10.1175/1520-0442(2002)015<1020:TOAWEA>2.0.CO;2.

Zhang, X., and F. Zwiers, 2004: Comment on ''Applicability of prewhitening to eliminate the influence of serial correlation on the Mann–Kendall test'' by Sheng Yue and Chun Yuan Wang. *Water Resour. Res.*, **40**, W03805, doi:10.1029/2003WR002073.